AUTOMOTIVE LEAD-ACID BATTERY

STATE-OF-HEALTH MONITORING SYSTEM

Ross Kerley

Thesis submitted to the faculty of the Virginia Polytechnic Institute and State University in partial fulfillment of the requirements for the degree of
Master of Science
In
Electrical Engineering

Chair: Dong S. Ha
Kwan-Jin Koh
Qiang Li

July 30, 2014
Blacksburg, Virginia

Keywords: Lead Acid Battery, State of Charge, State of Health

Automotive Lead-Acid Battery State-of-Health Monitoring System

Ross Kerley

ABSTRACT

This thesis describes the development of a system to continuously monitor the battery in a car and warn the user of an upcoming battery failure. An automotive battery endures enormous strain when it starts the engine, and when it supplies loads without the engine running. Note that the current during a cranking event often exceeds 500 Amperes. Despite the strains, a car battery still typically lasts 4-6 years before requiring replacement. There is often no warning of when a battery should be replaced and there is never a good time for a battery failure.

All currently available lead-acid battery monitoring systems use voltage and current sensing to monitor battery impedance and estimate battery health. However, such a system is costly due to the current sensor and typically requires an expert to operate the system. This thesis describes a prototype system to monitor battery state of health and provide advance warning of an upcoming battery failure using only voltage sensing. The prototype measures the voltage during a cranking event and determines if the battery is healthy or not. The voltage of an unhealthy battery will drop lower than a healthy one, and it will not recover as quickly.

The major contributions of the proposed research to the field are an algorithm to predict automotive battery state-of-health that is temperature-dependent and a prototype implementation of the algorithm on an ARM processor development board.

ACKNOWLEDGEMENTS

I would like to acknowledge and thank a number of people and organizations that have helped make this thesis a reality.

Dr. Dong Ha for providing me with the advice and support to see this project through.

Dr. Kwan-Jin Koh and Dr. Qiang Li for the commitment of their time and effort in support of my research.

Ji-Hoon Hyun for his neverending assistance with the batteries.

Interstate Batteries in Salem, VA for providing the batteries for this experiment.

Virginia Tech Fleet Services for initial battery measurements that started this work.

This work was supported by the Center for Integrated Smart Sensors funded by the Ministry of Science, ICT & Future Planning of Korea as Global Frontier Project (CISS-2-3).

My parents for always encouraging me to do the right thing, and for being proud of everything I have done.

My girlfriend Stephanie for all of her love and patience despite the distance between us, and my mind often wandering to batteries instead of our conversations.

TABLE OF CONTENTS

LIST OF FIGURES

LIST OF TABLES

1 INTRODUCTION

This thesis explores existing methods of automobile starting, lighting, and ignition (SLI) battery state of health (SOH) estimation. Additionally, it presents and tests a novel technique to estimate SOH. SLI batteries wear out after several years, but there is never a convenient time for them to expire. No advance warning is available in modern cars for an impending battery failure. SLI battery SOH monitoring would warn the driver that their battery has little life remaining, and that they should have their battery tested by a professional or replaced.

The strain applied to car batteries is increasing every year. Electrical loads in vehicles, such as entertainment systems and active suspension can require significant amounts of power that must be instantaneously supplied by the battery. As our cars become more advanced, these loads increase. Additionally, numerous cars that turn off the engine automatically instead of idling when stopped, such as at a red light, are coming to market. These are referred to as 'micro-hybrid' or 'stop-start' vehicles. This technology requires that the battery sustains all electrical loads frequently when the alternator is not supplying power, and it increases the frequency of engine starting. Starting the engine is still the most strenuous role for a car battery. During the cranking event, currents are on the order of several hundred amperes, greater than 1 kA for some vehicles [1].

Lead acid batteries are common and are used in automobiles for starting the engine and for running the lights and various electronics. They are also used in some electric vehicles such as golf carts and boats. In addition to mobile applications, they are used in battery backup systems for security systems, computers, and telephones. Additionally they are also found in alternative

energy systems for off-grid applications. Lead acid batteries are so prevalent because they use cheap and common materials and are easy to produce and recycle [2].

Lead acid batteries are a chemical system that stores energy. Discharging the battery converts the stored chemical energy into electrical energy that can be used to perform work. Two electrodes, Pb (Lead) and PbO_2 (Lead Oxide) are submerged in a solution of H_2SO_4 (Sulfuric Acid). $PbSO_4$ (Lead Sulfate) forms on both electrodes when discharging. When charging, lead sulfate is reduced to lead and lead oxide. This reaction is shown in (1) and Figure 1. The sulfuric acid solution is most concentrated when the battery is fully charged [2].

$$\underset{\text{Charged}}{Pb + PbO_2 + 2H_2SO_4} \leftrightarrows \underset{\text{Discharged}}{2PbSO_4 + 2H_2O} \tag{1}$$

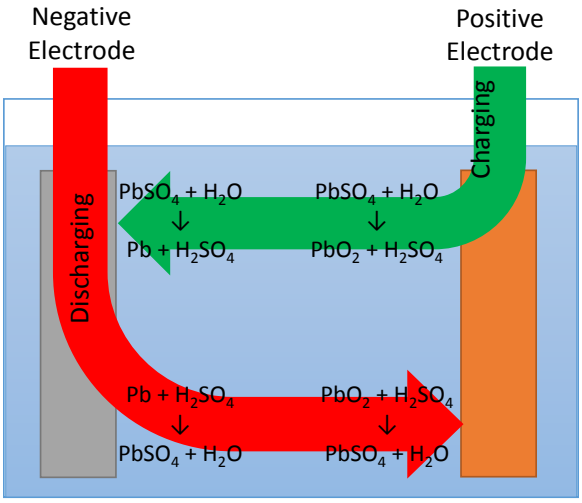

Figure 1: Simplified Chemical Reactions in a Lead Acid Battery

The cranking ability, or maximum discharging current of a battery, is directly proportional to the area of the lead plates, or electrodes, inside the battery. To maximize this current, which is needed to start a car, battery designs use gridded electrodes and thin electrodes in parallel. Batteries that require a high capacity generally have thicker plates to give more capacity. To

compensate for the reduced capacity due to the parallel thin plates, car starter batteries frequently have higher concentration acid solutions [1].

Electrical models of batteries have a wide range of complexity. The least complex models are merely an ideal voltage source, while the most complex consist of voltage sources and dozens of complex impedances. When simulating and predicting battery performance, the most simple model should be used to reduce complexity, but a minimum amount of accuracy is needed. For many purposes, a Thevenin-discharge model can be used. This model is shown in Figure 2. It requires four parameters: E_p, R_p, C, and R_o [3]. These parameters vary with the state of charge (SOC) of the battery, and also with the SOH. This model is quite simple, but for this work an even less sophisticated model is appropriate [3].

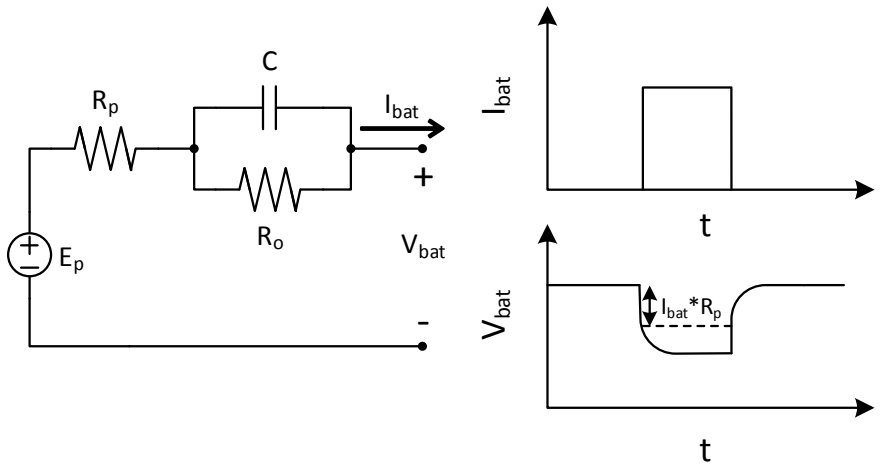

Figure 2:Thevenin-discharge battery model [3].

Grube presented that the impedance of a healthy battery during cranking is almost purely ohmic [4]. This was tested by taking the voltage and current waveforms during a cranking event, and plotting voltage versus current. These points and the resulting regression are shown in Figure 3. The open circuit voltage (OCV) or no-load voltage is indicated by V0 (intercept voltage). It is apparent that as various currents are drawn from the battery, the voltage is the result of almost

purely ohmic impedance. Therefore, the Thevenin-discharge battery model can be simplified as only E_p and R_p for a healthy battery [4]. In Figure 3, the battery resistance is approximately 0.004 Ω. With a 500 A load, the voltage drops by approximately 2 V.

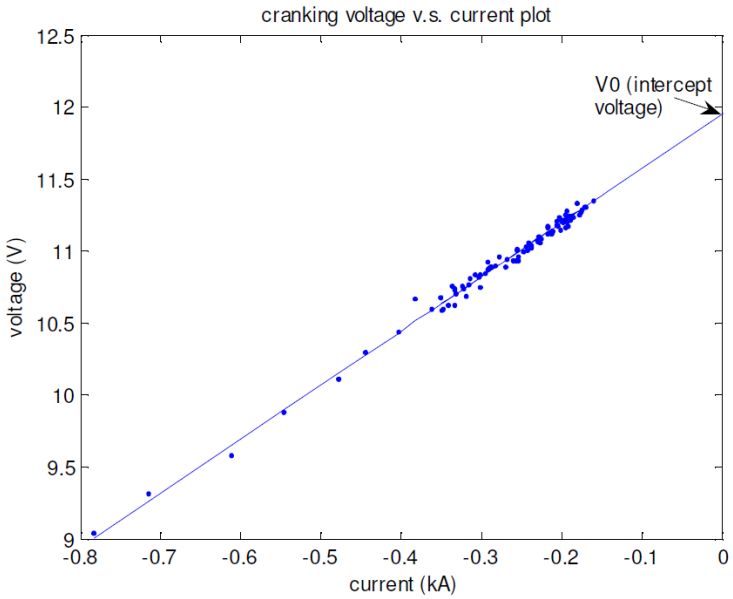

Figure 3: Extracted current and voltage waveforms as V-I plot [4]

There are several aging mechanisms that contribute to performance degradation and end of service life. These include anodic corrosion, positive active mass degradation, irreversible formation of lead sulfate, short-circuits, and loss of water. Of these five mechanisms, two are common in automotive starter batteries. The first, grid corrosion, is considered the most "natural" death for a lead acid battery. It is an expected failure mode when the battery is overcharged or held at a high State-of-Charge (SOC) for extended periods of time, such as when driving a long distance. The second common aging mechanism, positive active mass degradation, is accelerated by numerous shallow discharge cycles [5].

2 BACKGROUND

Lead acid batteries have been used in automobiles for many decades to start the internal combustion engine. A typical car battery lasts about five years before requiring replacement. However, they can wear out in as little as two years or last as many as ten years under ideal conditions. When a battery does reach the end of its service life, it is not at an ideal time and there is often no warning. Therefore, it is advantageous to monitor the battery health and warn the vehicle operator when a battery is near the end of its life [5], [6].

2.1 Quantifying State of Health in Lead Acid Batteries

Battery SOH is a quantification of a battery's electrical ability with regards to storing and delivering energy [7]. In batteries typically used for storage and slow delivery of energy, SOH is based on their capacity. This is a relatively simple quantification, which is simply the ratio of the current capacity and the designed capacity. This common method of determining SOH can be found in modern laptops and phones.

$$SOH_{capacity} = \frac{Current\ Capacity}{Designed\ Capacity} \tag{2}$$

SOH for car starter batteries is more complicated. Car batteries degrade in both capacity and current delivering ability. A battery could be discharged slowly and still release enough energy to be considered healthy according to (2). However, the battery is unhealthy if it cannot supply enough current to start the car.

2.2 Existing Methods Applicable to Car Battery SOH

There are several existing methods or systems which can be applicable to car battery SOH. The most relevant methods are described in this section.

2.2.1 Coup de Fouet SOH Estimation

Since 1964, a phenomenon known as *coup de fouet* has been identified and studied in lead acid batteries [8]. The term, French for whiplash, identifies the recovery of battery voltage after a load transient. This trait is easily seen when the battery is subject to a large and constant load. The voltage makes a sudden drop to a *trough voltage* when the load is first applied, and then it recovers to a *plateau voltage* after some amount of time, typically on the order of several minutes [9]. A measurement of this phenomenon and the Plateau and Trough voltages are shown in Figure 4.

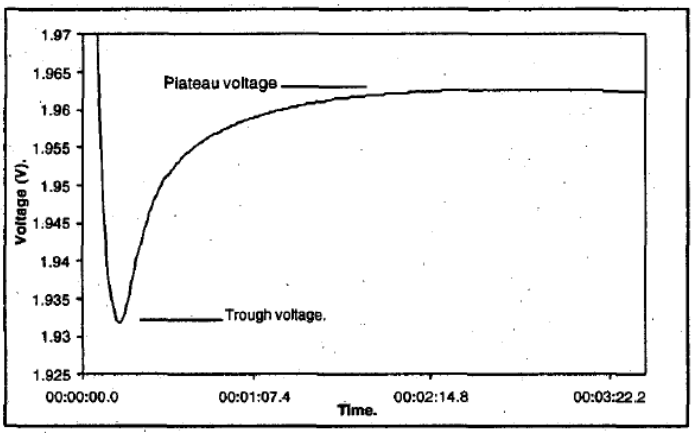

Figure 4: Coup de fouet of a Oldham 2HI275 cell discharged at 275A [9]

This trait has been studied in depth for many decades. In 1999, a method was proposed to relate *coup de fouet* to remaining battery capacity [9]. Pascoe and Anbuky provided experimental results that the parameters extracted from this region are useful in estimating battery capacity.

However, they explain that two minutes of constant discharge is necessary to determine the parameters. Additional work has been performed to extend this concept to State-of-Health and expanding its applications to battery capacity [10]–[12].

Due to the long measurement period, this technology is best applied to batteries that will experience constant loads for long periods of time, not the starting of a car. The starting of a car is over a period of a few seconds at most, and the current varies. Therefore, this technology is not applicable to car starter batteries.

2.2.2 Impedance Based SOH Estimation

There is a correlation between the impedance of a battery and SOH. One technique that exploits this correlation is called Impedance Spectroscopy. This technique measures battery impedance across a spectrum of frequencies. Battery impedance exhibits a strong correlation with age and wear. Numerous researchers have determined that impedance is worthwhile for battery SOH analysis [13]–[16].

Blanke et al present an approach to determine SOC, cranking ability, aging and modeling parameters using impedance spectroscopy [15], [16]. Their method measures the voltage and current of the battery during normal use. They utilize current and voltage ripples due to the loads and alternator instead of costly active excitation. The measured current and voltage ripples are processed to obtain the impedance at various frequencies. They determined that the most useful period of time for estimating SOH is during cranking and they have built a SOH monitor to do this. Vehicle testing of the monitor showed satisfactory results predicting SOH. The device must

have 10 mA current resolution over a range from 0.1 to 1000 A [15], [16]. This stringent requirement drives up the cost of a SOH monitor.

2.2.3 Battery Cranking Voltage Based SOH Monitoring Method

Grube investigated a voltage-only measurement to determine if a car starter battery needs replacement, needs charging, or is sufficient for use [4].

This work focused on observing the first two valleys present in the voltage waveform during a cranking event. As shown in Figure 5, the voltage of a healthy battery (top) increases from the first valley to the next. In contrast, an unhealthy battery's voltage decreases. This difference is due to the battery chemistry not keeping up with the required amount of current to start a car. As a result, even as the current required decreases, the voltage continues to fall for an unhealthy battery. In a healthy battery, the relationship between voltage and current is practically ohmic, and the battery could be modeled as a voltage source with a series resistor. An unhealthy battery has a more complex relationship as the voltage continues to drop even when the load is reduced.

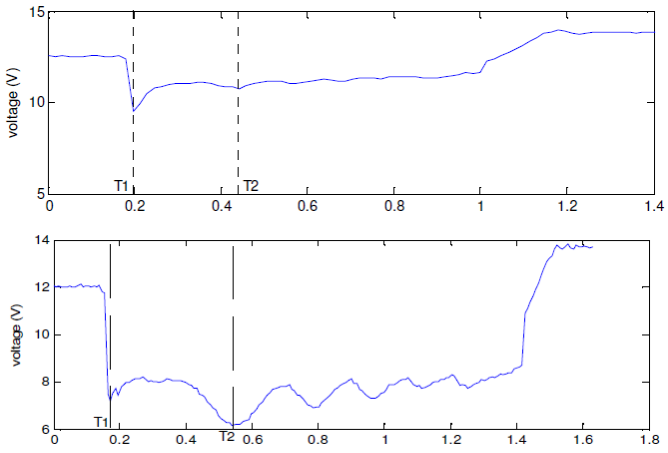

Figure 5: Typical Battery Voltage Waveforms During Cranking for a Healthy Battery (top) and an Unhealthy Battery (Bottom) [4]

Grube measured voltage and current and derived battery impedance during cranking of healthy and unhealthy batteries. These waveforms are shown in Figure 6. The healthy battery is on the left. Its voltage waveform, top-left, exhibits an initial valley, and then a much higher second valley. The current waveform, mid-left, exhibits similar valleys. The bottom-left graph shows the relationship between the voltage and current. The linear relationship enables one to obtain the voltage at the battery terminals by measuring the current, multiplying by a constant series resistance, and adding the initial OCV. The resistance derived from this graph is near 3 mΩ. The unhealthy battery has a different relationship. Its current waveform, mid-right, looks similar to the healthy battery with a second valley higher than the first. However, the voltage waveform, top-right, has a second valley which is lower than the first. The resulting plot of voltage against current, bottom-right, is no longer a linear relationship and the battery impedance can no longer be approximated as a resistor. It is concluded that if the second valley is higher than the first one, the battery is healthy. If the second valley is lower, it is a sign that the battery is weak and should be replaced [4].

Grube's proposed algorithm for estimating SOH compares the battery voltage when the starter is engaged (first valley) to the next local minimum voltage (second valley). SOH is inferred by comparing the difference between the two valleys (ΔV) with a threshold value from a lookup table. The voltage thresholds should be a function of temperature. Due to complexity, Grube used a fixed threshold of 0.7 V [4].

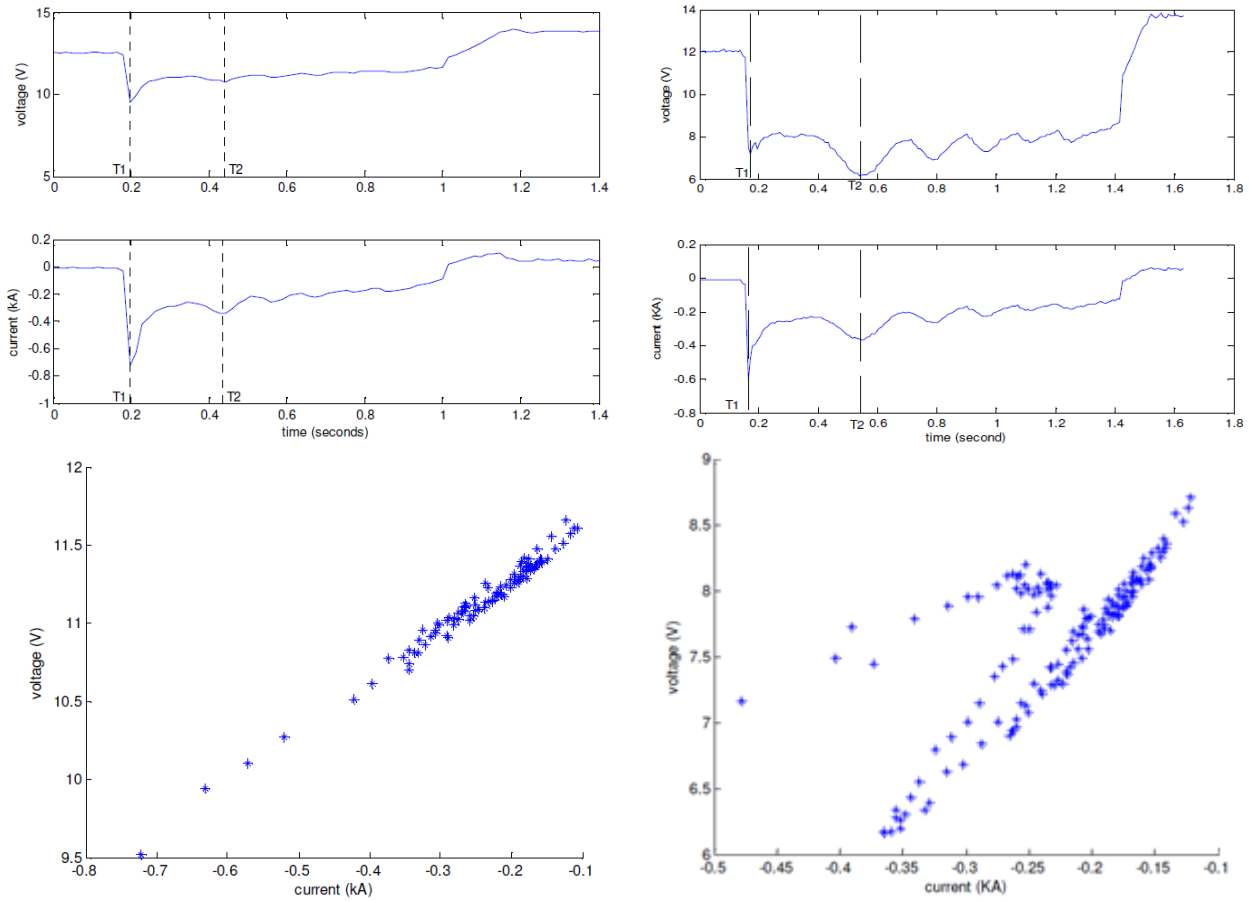

Figure 6: Voltage and Current Waveforms of healthy (left) and unhealthy (right) batteries [4]

In his results, Grube identified that this algorithm did provide a timely warning. However, he states that further improvements are needed to make it more reliable. Particularly, the lookup table of threshold voltages as a function of temperature should be populated. With the fixed threshold, a battery that is close to failure but is only tested when hot might not give any warning and then fail to start the car if the next crank occurs when it is cold [4].

2.2.4 Parity-Relation Based SOH Monitoring

To improve the previous SOH estimation algorithm, Grube also investigated a method that uses both voltage and current sensing. The method, called parity-relation, is based on the relationship between the voltage and current of healthy batteries which is obtained by measuring the terminal

voltage under various battery currents. One can estimate the voltage waveform of a healthy battery from a measured current waveform during cranking. The difference between the estimated and measured voltages is used to infer SOH. If the measurement differs greatly from the expectation of a healthy battery, the SOH of the battery is poor. An extensive part of the work in this method is characterizing healthy batteries. It employs V-I plots of cranking data, like those in Figure 6. Similarly, Figure 7 shows V-I data for a battery at various states of health [4], [17].

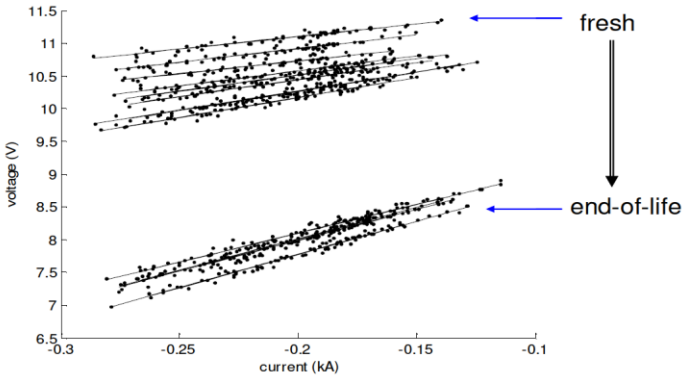

Figure 7: V-I plot of cranking data collected during battery aging process [4].

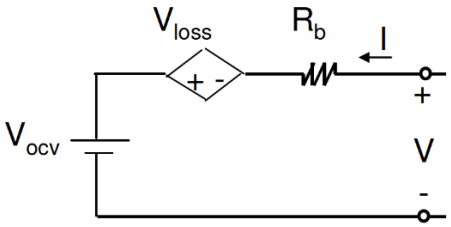

Figure 8: Battery model during cranking [4].

Figure 8 shows an approximate circuit model used by Grube. The parameters V_{loss} and R_b can be used to estimate the terminal voltage given a measurement of current. The data in Figure 7 was processed to extract V_{loss} and R_b for each battery test case. The extracted values are shown in Figure 9. After ten aging periods, there is a sharp increase in both parameters, V_{loss} and R_b. This sharp increase is related to the decrease in voltage near end of life in Figure 7 [4], [17].

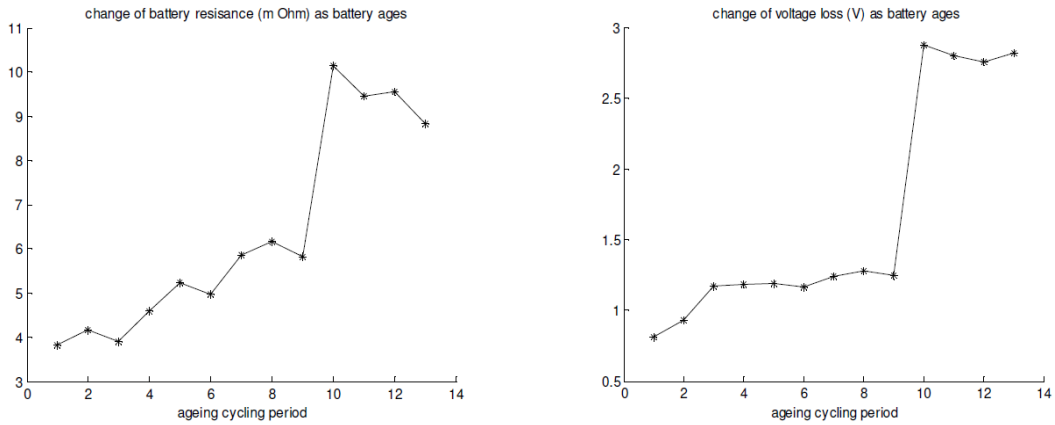

Figure 9: Battery model parameters as battery ages. Left: R_b, Right: V_{loss} [4].

2.2.5 Commercial In-car SOH Monitoring

Commercial solutions for battery SOH estimation rely on voltage, current, and temperature sensors. Numerous manufacturers have made all-in-one battery sensors available to car manufacturers. A car manufacturer can then implement a SOH estimation algorithm within the car's ECU (Engine Control Unit). A current sensor should be able to measure upwards of 1 kA (1000 A) and still have fine precision at low current levels. Battery current, voltage and temperature sensors are available from Bosch, Hella, Delphi and more [18]–[21].

The Battery Monitoring Device from Delphi shown in Figure 10 is interesting because it performs both SOC and SOH estimation. It is rated to measure currents as high as 1500 A using a 100 μΩ shunt. This monitoring device is able to reduce fuel consumption and extend battery usable life [21].

Figure 10: Delphi Battery Monitoring Device [21].

2.2.6 Commercial Out-of-car SOH Estimation

Commercial products exist for testing batteries with high precision. These testers are commonly used by repair technicians to assess the health of a battery to determine if an old battery has reached its end of life. Midtronics, a reputable producer of these testers, uses conductance testing to determine health [22].

Conductance is the real part of the complex admittance of a battery. This is essentially defining the ohmic behavior or a battery. Conductance decreases as a battery ages, and is directly related to the Cold-Cranking-Amp (CCA) rating of a starter battery. When the measured CCA has dropped to less than 75% of its rated value, the battery is considered to be at the end of its usable life. The Midtronics battery testers are considered the industry standard in determining battery condition. A Midtronics MDX-600 is shown in Figure 11 [22].

Figure 11: Midtronics MDX-600 Battery Analyzer [22]

2.3 Proposed Research and Contributions

There are several existing methods in the field of lead acid SOH estimation. The most accurate solutions require both battery current and voltage sensing to determine battery impedance [13]–[17], [21]. Utilizing current measurements allows simple and highly accurate SOH estimation. A voltage-only SOH estimation method was proposed in a previous work, but the method was not explored fully to achieve the desired performance [4]. This thesis research investigates a SOH estimation method for car batteries based on voltage measurements, which intends to improve the performance of the existing one [4] substantially. The objective of the proposed algorithm is to monitor an automotive battery's SOH and inform an operator of deteriorating health.

The major contributions of the proposed research to the field are:

- Completion of the algorithm presented in [4] by incorporating temperature-dependent thresholds. They were proposed in that work, but not completed.
- Enhancement of the algorithm presented in [4] by analyzing more points in the voltage waveform. Analyzing the initial voltage drop helps to more accurately predict battery end-of-life.
- A prototype implementation of the algorithm using an ARM processor development board. This prototype is capable of analyzing a battery's voltage during a cranking event and reporting to the driver whether the battery is healthy or not. It also serves as a data collection device that can record ambient temperature and voltage waveforms for later review.

3 PROTOTYPE STATE OF HEALTH MONITORING SYSTEM

This chapter describes the proposed algorithm for SOH estimation for car batteries and the prototype of the system. Determination of design parameters and hardware building blocks of the prototype are also described.

3.1 State of Health Estimation Algorithm

The proposed algorithm was built upon the voltage-only approach presented by Grube in [4]. The algorithm was originally prototyped in Matlab and tested using recorded voltage data obtained from a real car cranking. Once enhancements to the algorithm were made to improve its versatility and reliability, the algorithm was ported over to a microcontroller. After real-world testing, additional modifications and calibrations were performed. The algorithm presented here is the final algorithm that is implemented on a microcontroller.

3.1.1 Algorithm Overview

A block diagram of the algorithm is shown in Figure 12. It begins by waiting until the battery voltage has settled so that SOC can be estimated accurately. Once the battery voltage is settled, typically 30-60 minutes after stopping the car, the voltage becomes its OCV assuming the power dissipation while off is negligible. The SOC is estimated from a lookup table based on the OCV and the ambient temperature. Evaluation of the SOH proceeds only if the SOC level is above 60%. If SOC is below 60%, the user may be warned that they should drive more or charge their battery.

If the SOC is above 60%, the algorithm waits for a cranking event. If the SOC drops below 60% while waiting for a crank, the algorithm returns to the beginning. A cranking event is identified by the steep down-slope when the starter motor first engages. After the start of the cranking event, the algorithm identifies the first two local minima (valley voltages). Once identified, the algorithm waits to see if the car starts within several seconds. This is signified by the battery voltage rising above 13 V. Once successfully started, it determines the SOH based on OCV, SOC, the two valley voltages and ambient temperature. If the battery is unhealthy, the user (driver) will be notified to get their battery tested or replaced.

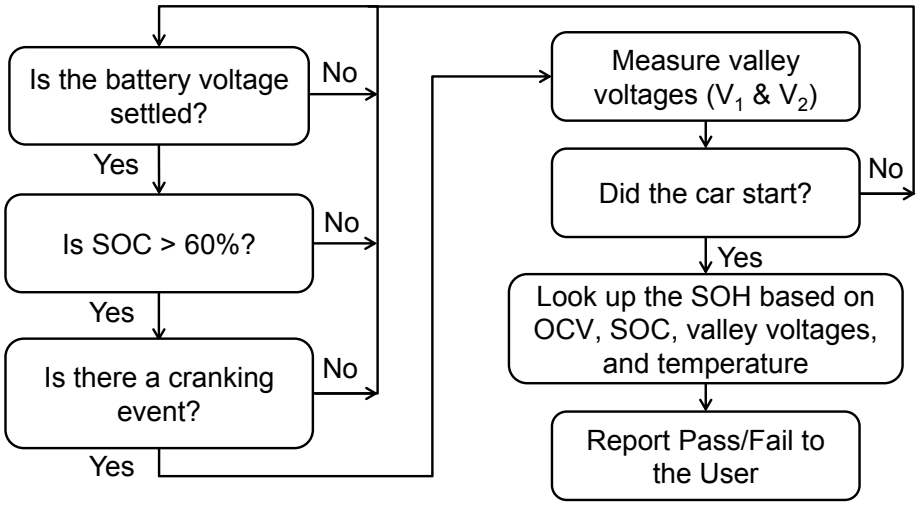

Figure 12: Decision Path for SOH Algorithm

The SOH estimation algorithm consists of several components. The algorithm includes voltage sampling, state of charge estimation, valley detection, real time clock Interfacing, SD card data logging, temperature measurement, and SOH estimation. For the sake of brevity, only the most relevant components will be discussed in detail in the following subsections.

3.1.2 State of Charge Estimation

The SOC estimation method chosen for the proposed algorithm relies on the battery OCV. It is important to note that the battery terminal voltage of a car may never reach its OCV as some amount of current is perpetually drawn from or pushed to the battery. A true OCV requires the current in or out of the battery to be zero for an extended amount of time, on the order of hours. Despite this, the terminal voltage of the battery is practically the OCV. For example, the maximum current to be expected when the car is not in operation is 50 mA [23]. The battery resistance derived from Figure 6 is approximately 3 mΩ. The voltage drop with a 50 mA load is only 150 μV. The SOC error is then much lower than 0.1%.

The minimum settling time for OCV is thirty minutes at 25 °C. At lower temperatures, that minimum time increases. For this algorithm, the battery voltage is considered settled when there is no more than a 0.1 V change within 60 minutes. This is calculated by comparing the maximum voltage within 60 minutes to the minimum voltage in the same period.

In lead-acid battery chemistry, the OCV relates directly to the acid concentration of the electrolyte. This relationship is well established and agreed upon, as shown in Figure 13. This figure shows three sets of OCV vs relative density measurements and two sets of calculations at 25 °C [2]. Table 1 is constructed from the values extracted from Figure 13. These values are used in the algorithm for SOC estimation. Note that a car battery has six cells connected in series and the OCV of a battery is six times that of a cell.

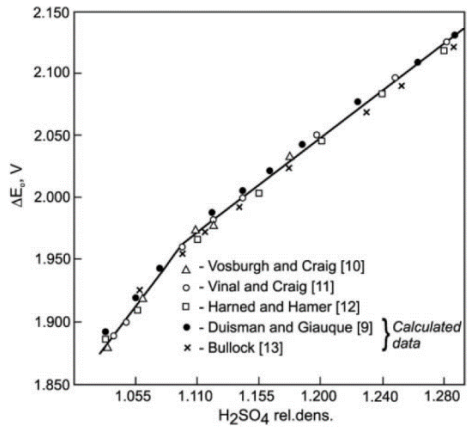

Figure 13: Lead-acid cell voltage at 25 °C as a function of H_2SO_4 relative density [2]

Table 1: Lead-Acid Cell Voltage vs Specific Gravity of H2SO4 Electrolyte [2]

S.G.	V_{cell}
1.030	1.876
1.051	1.907
1.068	1.932
1.081	1.951
1.089	1.963
1.104	1.976
1.119	1.989
1.137	2.004
1.152	2.016
1.169	2.030
1.186	2.045
1.202	2.058
1.216	2.071
1.232	2.083
1.248	2.097
1.262	2.110
1.278	2.122
1.293	2.135

The battery OCV is not only a function of relative density (also known as specific gravity), but also of temperature. The temperature coefficient of OCV as a function of relative density is shown in Figure 14 [1]. At a given electrolyte relative density, the OCV can be calculated with the following equation.

$$OCV = 6 * [V_{cell}(S.G.) + [T_{amb} - 25] * T.C.(S.G.)] \quad (3)$$

Due to the nonlinearity of the temperature coefficient curve, a recursive approach is used to calculate battery electrolyte relative density. First, OCV is used to look up an approximate relative density from Table 1. Then, the approximate relative density is used to determine the temperature coefficient. The product of the ambient temperature and the temperature coefficient is subtracted from the measured OCV to determine what the OCV would be, if the battery was at 25 °C. This new OCV is used with Table 1 to determine the electrolyte relative density.

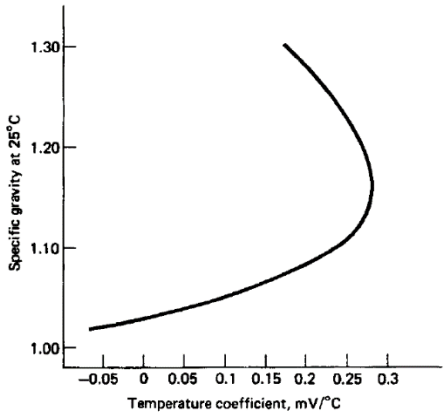

Figure 14: Temperature Coefficient of Open-Circuit Voltage of Lead-Acid Cell as a Function of Electrolyte Specific Gravity [1]

Though the relationship of OCV to relative density, also known as specific gravity, is highly agreed upon, this does not necessarily translate to simple SOC estimation.

Lead acid batteries are specifically designed for various applications. The most obvious difference between the types of batteries is their designed acid concentration which is proportional to relative density. Linden's Handbook of Batteries includes a table of common lead acid battery chemistries. It is reproduced in Table 2 [1]. Automotive SLI batteries have a moderate acid concentrations. Deep cycle batteries for electric vehicles have the highest concentration while deep cycle batteries for stationary applications have the lowest concentration. Column C, SLI battery, is used in this research.

Table 2: State of Charge vs Specific Gravity of Lead-Acid Batteries [1]

	Specific Gravity			
State of Charge	A EV battery	B Traction battery	C SLI battery	D Stationary battery
100%	1.330	1.280	1.265	1.225
75%	1.300	1.250	1.225	1.185
50%	1.270	1.220	1.190	1.150
25%	1.240	1.190	1.155	1.115
0%	1.210	1.160	1.120	1.000

The precise SOC is linearly interpolated using the estimated specific gravity and column C, SLI battery, of Table 2.

3.1.3 Voltage Sampling

The battery terminal voltage is sampled at 200 Hz with a 12-bit analog to digital converter (ADC). The resolution and the sampling rate are sufficient to correctly identify cranking waveforms. Ten seconds of data totaling 28 KB is stored in RAM.

If the battery voltage is settled and the car is off, the algorithm continuously samples and processes data. Every five seconds, the prototype processes the previous ten seconds of data. In this manner, every crank (that takes less than five seconds to complete) will be processed. This has been found to be sufficient for all batteries and vehicles tested. This may need to be increased in the future to accommodate a wider variety of cranking waveforms, or it could be reduced to utilize less memory space.

When data is processed, it copies the samples to a new array, so that this data is not disturbed while the microcontroller continuously samples. Then, a running average of four measurements is performed to filter out noise, which effectively eliminates false valleys. The prototype also stores the sampled time for each data point, which aids in examination of the data later. The

timestamps could be removed in future adaptations of this algorithm when most data logging will be unnecessary. Table 3 shows a summary of memory usage by the large arrays. The total memory usage by these arrays is 28 KB, which could be reduced to only 12 KB by eliminating the timestamps.

Table 3: Estimates of memory usage.

Variable	Size	Size	Notes
Voltage Sample	2000*16 bits	32 kbits	
Copied Voltage Sample	2000*16 bits	32 kbits	
Average Voltage Sample	2000*16 bits	32 kbits	
Sample Timestamp	2000*32 bits	64 kbits	Only for data logging
Copied Sample Timestamp	2000*32 bits	64 kbits	Only for data logging
Total Size		224 kbits	**28 Kbytes**

3.1.4 Slope Detection

The algorithm identifies the beginning of a cranking event by looking at the difference between two consecutive samples which are the rolling average of four samples. If the difference between two consecutive samples is greater than 0.25 V, a crank is detected and the algorithm will move on to valley detection. The samples are taken at 200 Hz, so 0.25 V equates to 50 V/s. Typical cranking waveforms exhibit a voltage slope in excess of 100 V/s. Figure 15 shows a voltage waveform during a typical crank. Example measurements and their slopes are shown in Table 4. These measurements are taken at the 12 V socket inside the passenger compartment of the car by the MCU, through a first-order RC filter. The filter is discussed in Section 3.1.7.

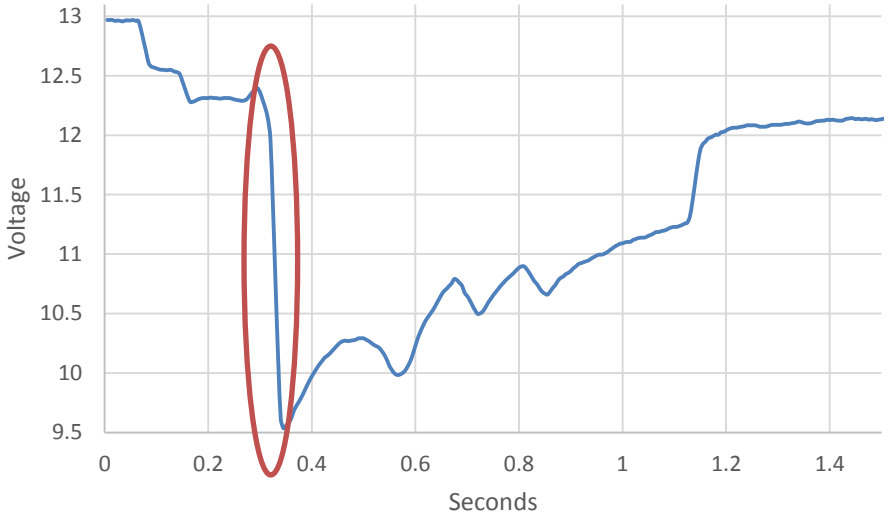

Figure 15: Typical cranking waveform

Table 4: Individual voltage samples during crank from the circled region of Figure 15.

Voltage (V)	ΔV (V)	Slope (V/s)
12.22925	-0.06719	-13.4387
12.14229	-0.08696	-17.3913
11.97233	-0.16996	-33.9921
11.39526	-0.57708	-115.415
10.74308	-0.65217	-130.435
10.11858	-0.62451	-124.901
9.616601	-0.50198	-100.395
9.537549	-0.07905	-15.8103

3.1.5 Valley Detection

Once a cranking event has been identified, the next step is Valley Detection. Valley Detection identifies the local minima in the voltage waveform. The algorithm identifies these by locating a sequence of 5 samples V_1, V_2, … V_5, which satisfy the following conditions.

$$V_2 < V_1 - 2.5\,mV$$

$$V_3 < V_2 - 2.5\ mV$$

$$V_4 > V_3 + 2.5\ mV$$

$$V_5 > V_4 + 2.5\ mV$$

Two examples are shown in Figure 16. The left plot, the first valley, has a much steeper slope than the second valley (right plot) but both satisfy the conditions.

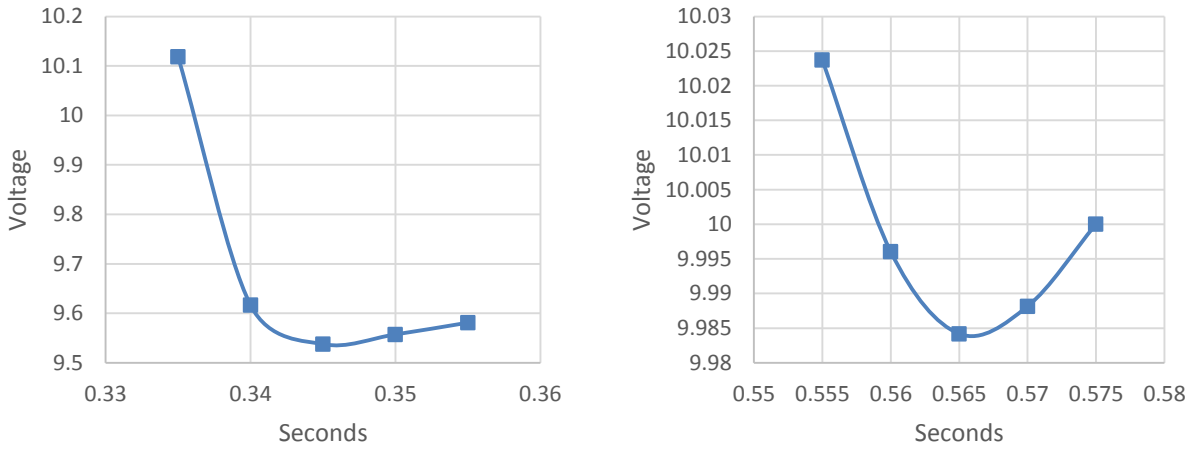

Figure 16: First and second valleys from the waveform given in Figure 15.

Once the first valley has been identified, the algorithm continues to process data to identify a second valley. Once found, the algorithm continues to the State-of-Health (SOH) Estimator.

3.1.6 State of Health Estimation

The proposed SOH Estimator uses the OCV, SOC, first valley voltage (V_1), second valley voltage (V_2) and temperature (T). The difference between the OCV and V_1 is denoted as ΔV_1. Note that ΔV_1 is the large voltage drop due to the starter motor of the engine engaging. V_2 minus V_1 is denoted as ΔV_2. These are indicated in Figure 17.

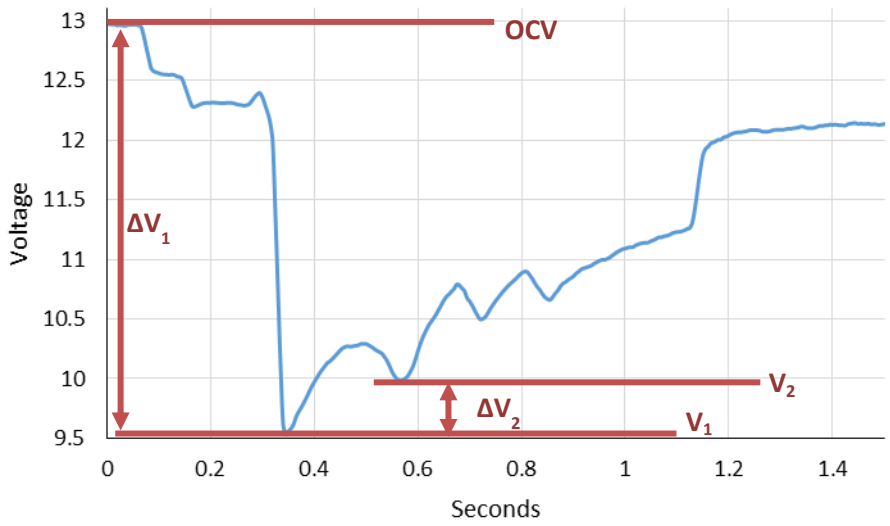

Figure 17: Typical Cranking Waveform for SOH Estimation

Grube's method estimates SOH using only ΔV_2 [4]. The method presented in this thesis takes into account temperature, ΔV_2, and ΔV_1.

3.1.6.1 Temperature Consideration

First, a threshold for ΔV_2 is retrieved from a lookup table using temperature. The value is linearly interpolated between table breakpoints and it defines the minimum ΔV_2 for a battery to be considered healthy. This temperature variance allows for the slower chemical reactions when a battery is cold. Setting the threshold higher when the battery is hot prevents a battery from passing consistently at high temperatures but then failing if it is operated in cold weather. Thresholds are listed in Table 5. These thresholds were developed experimentally by comparing the performance of the aged batteries. The values below 0 °C are estimated.

Table 5: V_{th1} across temperature.

Temperature (°C)	-30	-20	-10	0	10	20	30	40	50
V_{th1} (mV)	0	50	100	200	300	400	400	400	400

3.1.6.2 ΔV_1 Consideration

The next step is to consider ΔV_1. If ΔV_1 is very small, it is okay for ΔV_2 to also be small. Similarly, if ΔV_1 is excessive, the battery is likely unhealthy regardless of ΔV_2. Typical cranking performance showed a ΔV_1 of approximately 3 V. With this table, a V_{th} component is introduced that will raise or lower the threshold voltage to correct for ΔV_1. Values for V_{th2} are shown in Table 6. The values were developed experimentally by examining data from battery tests.

Table 6: V_{th2} with various ΔV_1

ΔV_1 (V)	1	1.5	2	2.5	3	3.5	4	4.5	5
V_{th2} (mV)	-160	-125	-90	-55	-20	15	50	85	120

3.1.6.3 ΔV_2 Consideration

V_{th1} and V_{th2} are added together to obtain V_{th}. Equation (4) shows the computation of V_{th}.

$$V_{th} = V_{th1}(temperature) + V_{th2}(\Delta V_1) \quad (4)$$

This complete threshold is compared to the measured ΔV_2. If ΔV_2 exceeds V_{th}, the battery is considered healthy. If ΔV_2 is less than V_{th}, the battery is considered unhealthy.

3.1.7 Example SOH Estimation

The procedure to obtain the SOH Metric is illustrated using example data shown in Table 7. First, measurements are taken of temperature, OCV, V_1 and V_2. Then, ΔV_1 and ΔV_2 are calculated from the voltage measurements. V_{th1} is obtained from the temperature value and the lookup table given in Table 5. The precise value is determined through linear interpolation of the

table breakpoints. Then, V_{th2} is obtained using ΔV_1 and a linear interpolation of Table 6. V_{th} is the sum of V_{th1} and V_{th2}. ΔV_2 minus V_{th} is considered our SOH Metric. If this metric is positive, the battery is healthy. Otherwise, the battery is unhealthy.

Table 7: Example SOH calculations. (Subset of Table 8)

Measurements					ΔV		Calculated Thresholds			SOH Metric
Date	°C	OCV	Valley 1	Valley 2	ΔV_1	ΔV_2	V_{th1}	V_{th2}	V_{th}	$\Delta V_2 - V_{th}$
June 22	30	12.80	8.72	9.29	4.08	0.56	0.37	0.06	0.42	0.14
July 2	37	13.00	8.52	8.96	4.48	0.44	0.41	0.08	0.50	-0.05

3.2 Hardware Prototype

The prototype consists of a software algorithm and various components that come together to make a functional State of Health estimation system. This standalone system can indicate if a battery is near failure through the use of indicator LEDs.

To aid in performance assessment, much of the sampled data should be stored for review. A SD card reader has been built into the prototype to enable data logging. To aid in identifying and storing data, a Real-Time-Clock (RTC) module is also integrated with the prototype. The algorithm requires battery voltage measurement and temperature, so an ADC and a temperature sensor are also required.

The prototype is shown in Figure 18. The (red) carrier board is a TI Launchpad with a TI TM4C1294NCPDT ARM Cortex M4 microcontroller [24]. This has 256 KB of RAM and runs at

120 MHz. With this algorithm, the microcontroller is significantly more powerful than required. The RTC, SD card, temperature sensor, and DC input header are identified in Figure 18.

The DC input header is found in Figure 18 at circle "A", which also includes a voltage divider and low pass filter. The divider is composed of 10 KΩ and 39 KΩ resistors for a divider ratio of approximately 1/5. A 0.47 μF capacitor is in parallel with the 10 KΩ resistor to create the low pass filter.

Circle "B" of Figure 18 is an SD memory card for data logging. Though not necessary for a final design, data logging was paramount for testing the algorithm. Circle "C" is a Real-Time-Clock module. This module supports a DS1307 I^2C Real-Time-Clock module and incorporates a backup battery to maintain the clock for years [25]. A RTC module is not necessary for the algorithm itself, because it should always have power. However, it is integral to data logging when power is disconnected. One modification had to be performed on the module. The DS1307 requires 5 V for operation, but the MCU only has a 3.3 V I^2C bus. The I^2C pull-up resistors on the RTC module are connected to 3.3 V, while the DS1307 still receives 5 V power.

Circle "D" of Figure 18 is an analog temperature sensor. The LM34 Fahrenheit Temperature sensor requires a 5 V supply and outputs an analog signal proportional to the ambient temperature [26]. This analog signal is directly connected to an ADC of the MCU which does not allow negative temperature operation. A different configuration or sensor is necessary to facilitate negative temperatures. In addition, locating the temperature sensor on the prototype in the passenger compartment is not ideal. It would be more helpful to have the temperature sensor at the battery, or at least in the engine compartment.

Circle “E” of Figure 18 contains the indicator LEDs. These four LEDs indicate when the OCV is being checked, when the OCV is stable and SOC has been measured, when a successful crank has been detected, and if the crank passed.

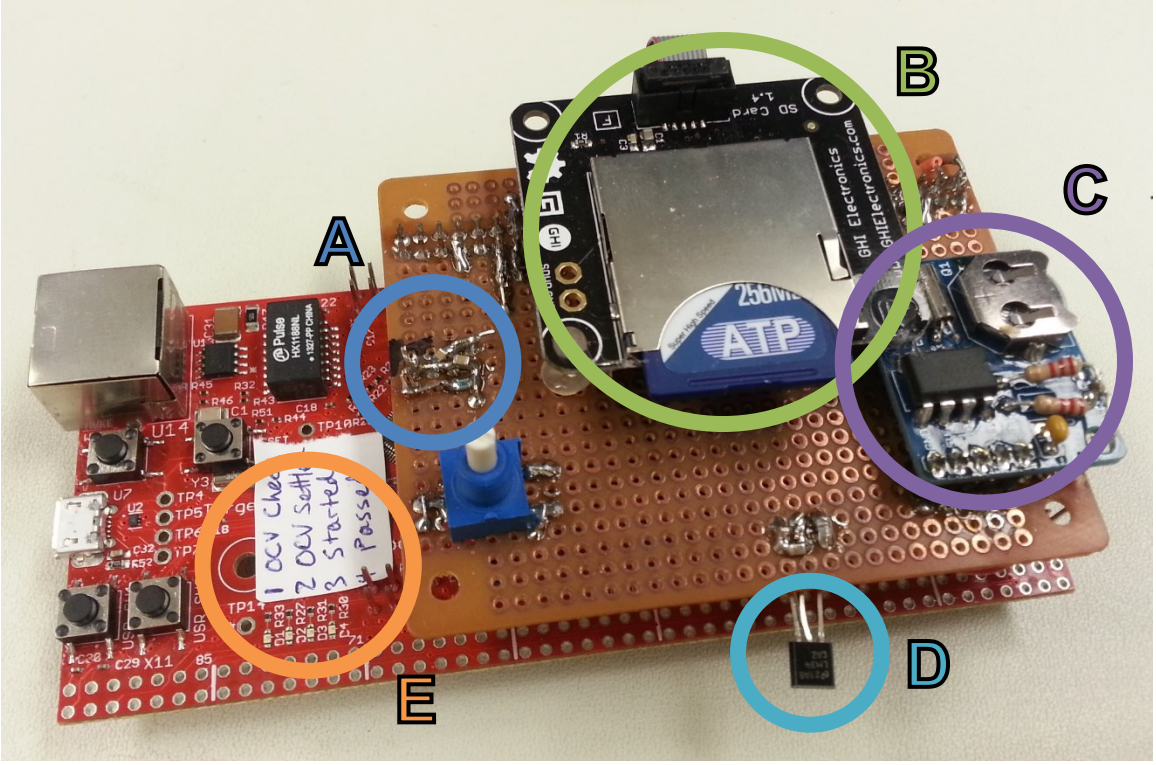

Figure 18: ARM development board with daughterboard.

A: DC input and LPF, B: SD card, C: RTC Module, D: Temperature Sensor, E: Indicator LEDs

4 TESTING PROCEDURE AND EXPERIMENTAL RESULTS

This chapter describes the procedure and the hardware for testing batteries and the prototype. It also describes the results obtained through testing.

4.1 Testing Procedure

Data from many batteries at various states of health is necessary to develop accurate thresholds and to verify correctness of the algorithm. To obtain this data, many batteries need to be aged and tested occasionally until they fail to start a car. To conserve time, an accelerated aging procedure is used. A widely accepted procedure known as "J240: Life Test for Automotive Storage Batteries" was published by the Society of Automotive Engineers [27]. For this research, a modified version of the procedure was used.

The specification recommends that the batteries are held at 75° C for the duration of the aging and testing. It recommends a ten minute charging period, and then a four minute discharge period. No more than a ten second delay is allowed between the charging and discharging phases. The procedure repeats for 100 hours between testing which consists of drawing the battery's rated current and verifying that the voltage does not drop too low. If battery passes the test, it repeats the 100 hours of aging and the test. The purpose of the whole procedure is to determine if a battery meets its specifications [27].

In order to accommodate a delay of less than ten seconds and to use a minimal amount of resources, the procedure was modified to include a five minute discharge period, along with the ten minute discharge period. This means that three batteries can share one load. At any point in

time, two batteries are charging while the third is discharging. After a complete 100 hour aging cycle, each battery was installed in a passenger car and a voltage waveform was recorded while starting the engine. In this manner, the testing could be used to verify the battery's health and to obtain voltage waveforms to fine-tune pass/fail thresholds.

4.2 Battery Aging Testbench

Ten batteries were aged and tested for this research. This section discusses the testbench to age the batteries.

4.2.1 Requirements

The requirements of the testbench to age the batteries in this thesis research were derived from SAE J240 [27]. The adapted requirements are:

- Maintain batteries at 75° C for the duration of the test.
- Repeatedly charge batteries to 14.8 V with no more than 25 A for 10 minutes at a time.
- Repeatedly discharge batteries with no more than 25 A for 5 minutes at a time.
- Charge and discharge ten batteries in 15 minute cycles for up to 100 hours.
- Record the current and voltage from each battery for later processing.

4.2.2 Hot Water Bath

J240 suggests using a hot water bath at 75° C to accelerate battery aging. A colder bath, 41° C, could be used but the number of cycles before failure would increase. Therefore, 75° C is used in this research.

A large stock tank was used to contain all 10 batteries and water [28]. Small bricks were used to lift the batteries off the floor of the tank and increase the water volume. This increase in volume helps temperature stability and water circulation. In addition, the bricks allowed some variance in battery height. Shorter batteries were raised up to be closer to the height of taller batteries. An off-the-shelf temperature controller and a thermocouple were used with a 1.2 kW plug-in heater to keep the water at 75° C. Foam insulation was crucial in maintaining the temperature and a lid reduces evaporation and more heat loss. The stock tank, insulation, and batteries can be seen in Figure 19 and Figure 20.

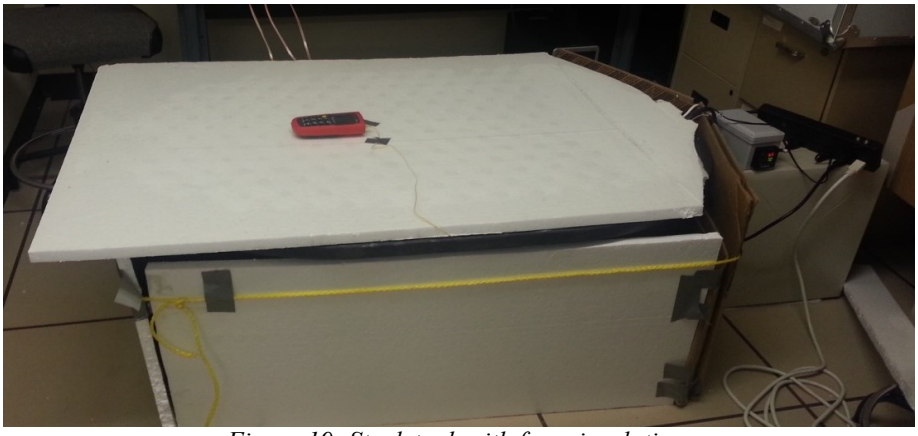

Figure 19: Stock tank with foam insulation.

Figure 20: Open stock tank with nine batteries and large heater.

4.2.3 Battery Charging and Discharging

A custom made load controller performs charging and discharging of three batteries simultaneously. A load controller is composed of a DC power supply, a 0.5 Ω 300 W resistor, and a controller to charge and discharge three batteries. The DC power supply for charging and the resistor for discharging are shared among the three batteries. Figure 21 shows the circuit board, power supply and resistor. Four of these setups are required for ten batteries because each one ages at most three batteries.

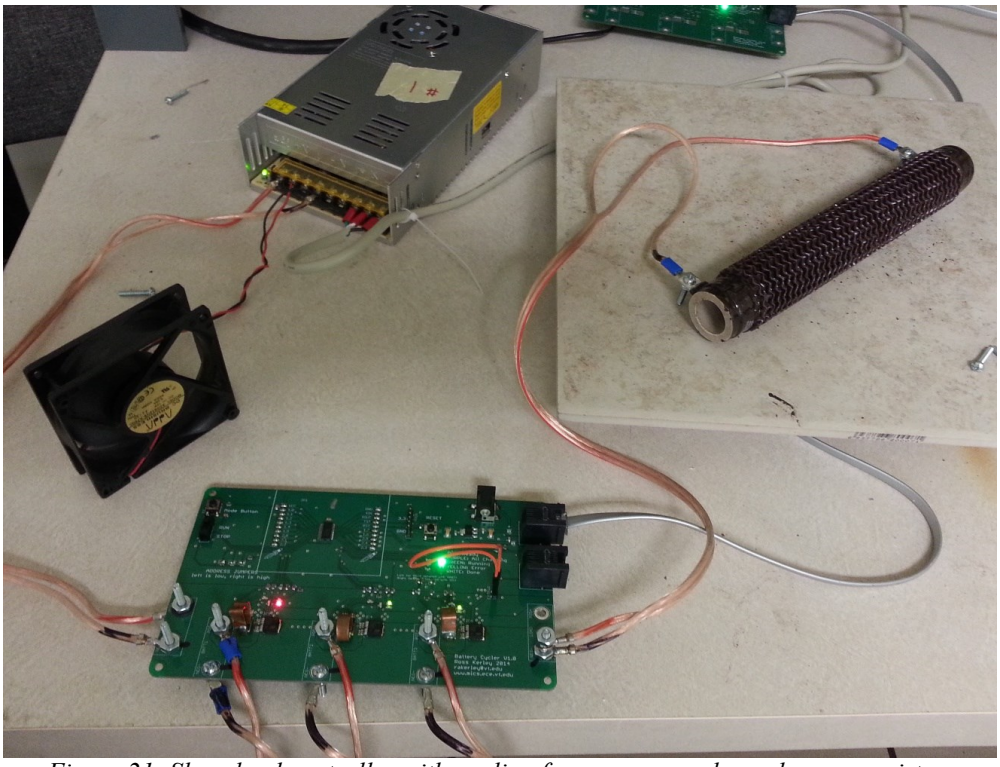

Figure 21: Slave load controller with cooling fan, power supply, and power resistor.

The custom PCB contains a TI MSP430G2553 microcontroller, indicator LEDs, and six STM VN5E010MH-E [29] load switch. The microcontroller actuates the load switches in sequence to charge or discharge each battery. It should be noted that two batteries are charging and one battery is discharging at any point in time. I^2C bus connectors are on each PCB so that they can

be networked for data logging. A block diagram of the load controller is given in Figure 22. This diagram shows the central microcontroller which actuates load switches to either charge each battery from 14.8 V or discharge it through a 0.5 Ω resistor. Voltage and current sensing for each battery are measured by the ADC on the microcontroller. An RGB LED gives user feedback, while a mode switch allows the user to start or stop the aging process.

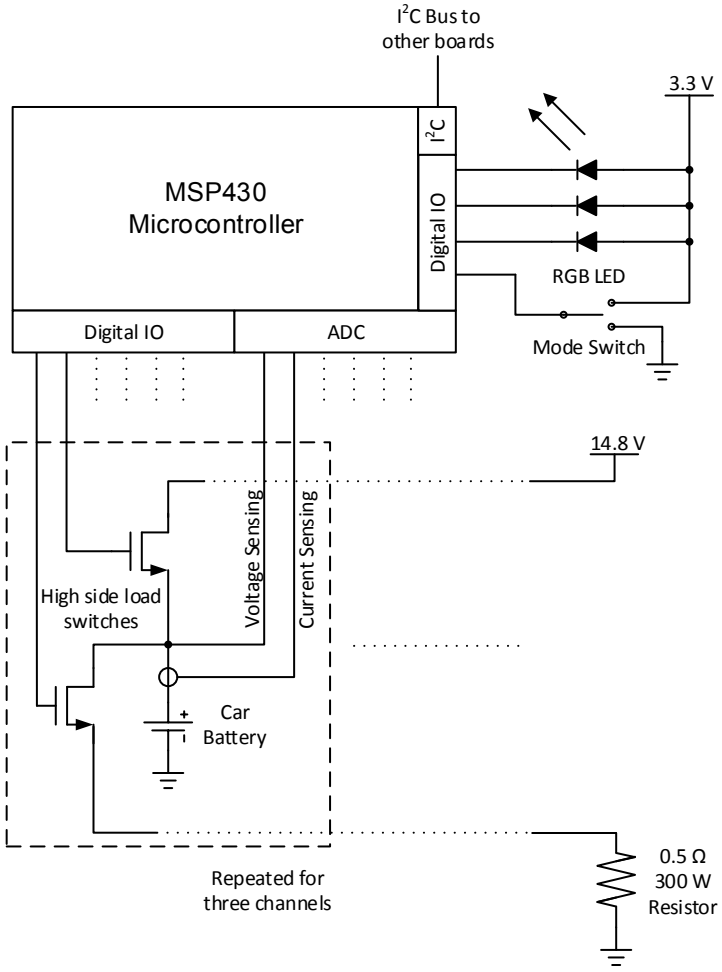

Figure 22: Block diagram of load controller

The master load controller, pictured in Figure 23, is responsible for I^2C communications with each load controller and serial communication over USB with the host PC.

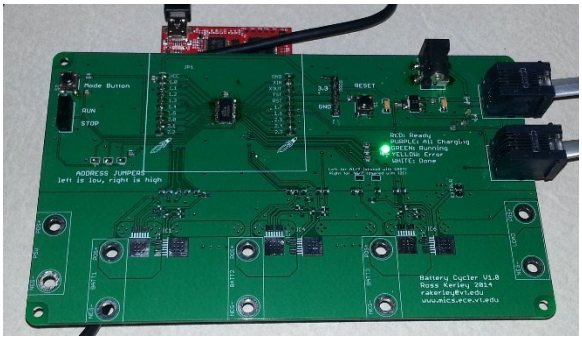

Figure 23: Master load controller.

A diagram of the connectivity between various components of the system is shown in Figure 24. The master load controller is connected to a computer through a USB to serial converter. The master controller polls each load controller through I^2C and requests current and voltage measurements. The values are stored on the host PC by a serial terminal program for later review. Software configurations for all the load controllers were developed in the Energia environment. The current system has one master load controller and four load controllers, which age ten batteries simultaneously.

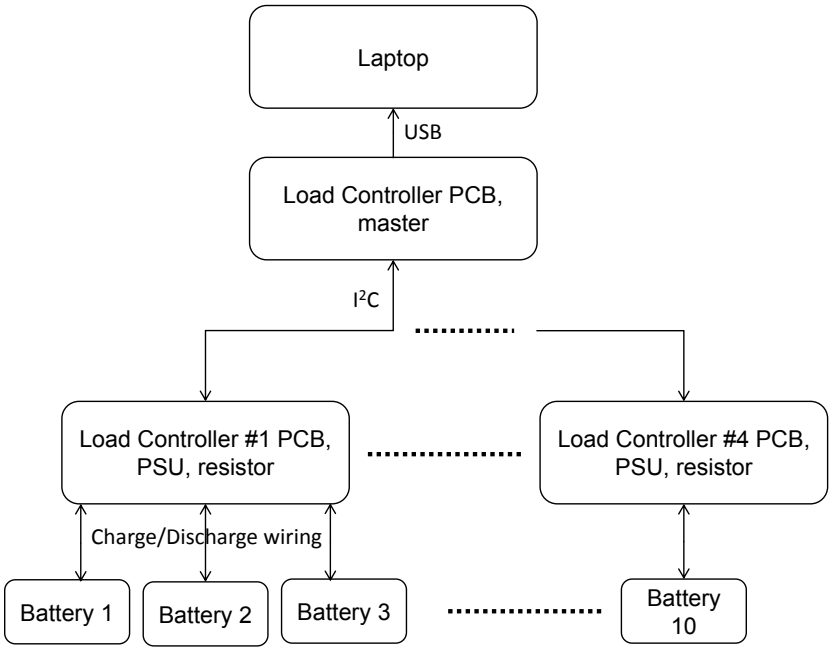

Figure 24: Block diagram of battery aging testbench

4.2.4 Data Logging

The master load controller receives current and voltage measurements from associated load controllers and send them to the host PC, which stores them later review. Example data, i.e., the battery voltage and current measurements, is shown in Figure 25. When the battery is charging, the voltage (top graph) is about 14 V, and the current (bottom graph colored green) flows into the battery. When the battery is discharging through the 0.5 Ω resistor, the voltage drops to about 8 V, and the current (colored red) flows out of the battery.

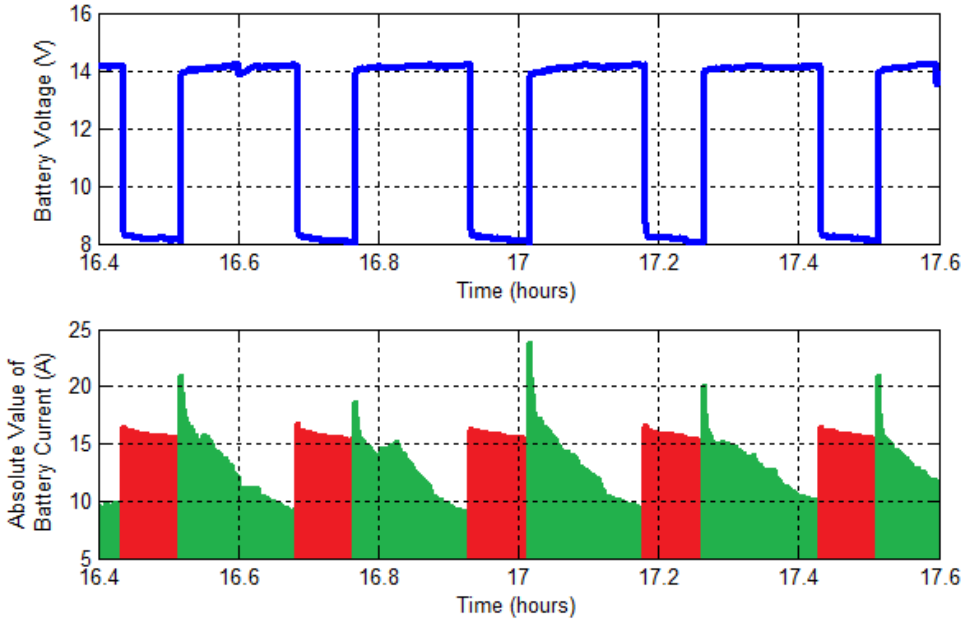

Figure 25: Graphed data log of charging and discharging a battery

4.3 Test Cranking

After each 100 hours of aging a battery, the battery is fully charged and then installed on a car and tested by starting the car. During testing, a USB oscilloscope (Digilent Analog Discovery) was used to measure and record the voltage waveforms in addition to the SOH estimator

prototype's own data logging. The USB oscilloscope is configured to sample at 10 kHz to allow sufficient resolution for post-processing of data. The sampling rate of 10 kHz is the maximum that does not cause a buffer overflow during recording. In addition to the USB oscilloscope, a laptop and thermometer are required for recording data and measuring temperatures. This equipment can be seen with a car in Figure 26.

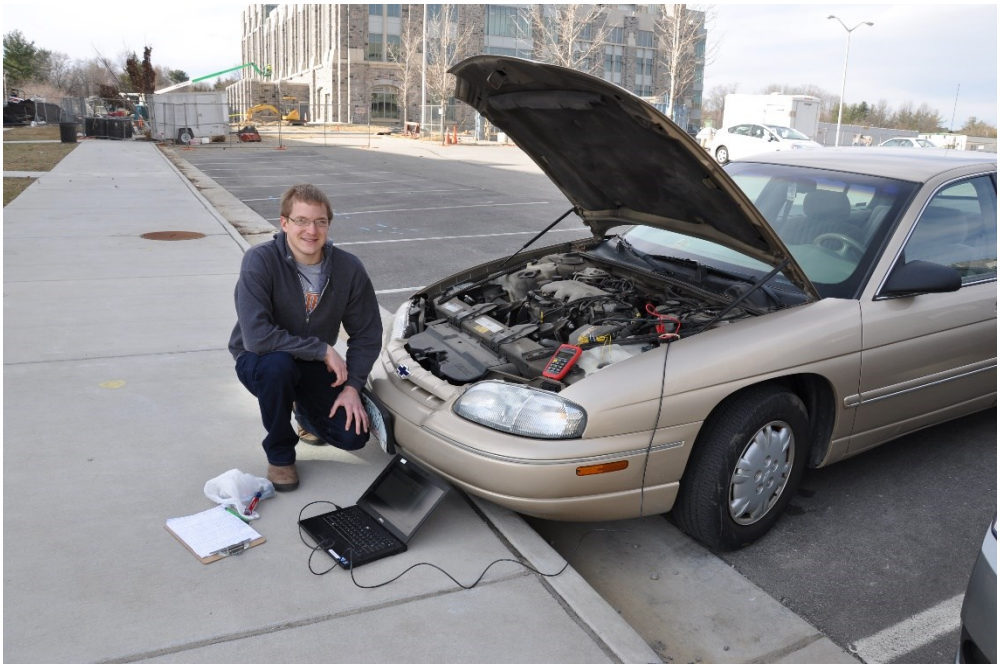

Figure 26: Testing the battery of a car

The proposed SOH estimator is connected inside the car's passenger compartment for monitoring voltage and measuring the temperature while cranking. This can introduce slight voltage loss between the battery terminals and a 12 V socket inside the car. Figure 27 shows a comparison of these two voltages. The MCU measured cranking waveform exhibits a 0.15 V difference from the terminal voltage measurement. It is largely due to resistance in cabling, and current drawn by car peripherals such as lighting, stereo, fans, and the SOH estimator itself. Resistance can be found in fuses, relays and the wiring. The voltage disparity causes a 15-20 % reduction in estimated SOC. To minimize this error, voltage should be sensed as close to the

battery as possible. Ideally, the SOH estimator system would be located inside the engine compartment directly connected to the battery.

Although this measurement error is apparent, its effects are insignificant. SOC is only used to determine if the SOH estimation can be performed. Voltage measurements used by the SOH estimator are relative, so the near-constant difference has no effect on ΔV_1 or ΔV_2. This can be observed in Figure 27. A slight offset could be incorporated to simply correct the error for SOC estimation if necessary.

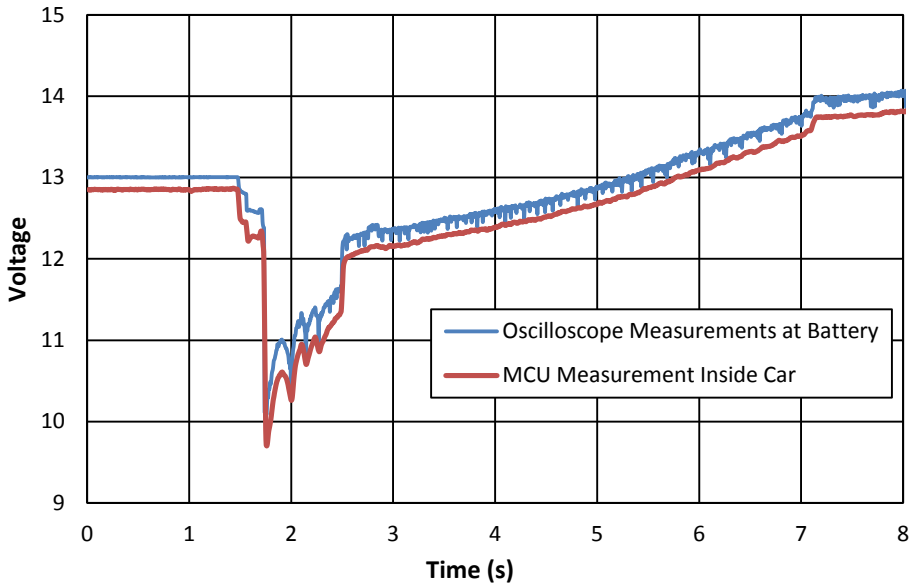

Figure 27: Comparison of battery terminal and MCU measurements

4.4 Results

The objective of this algorithm is to predict battery failure without sensing battery current during cranking. Collected waveforms from each crank test are analyzed to extract the relevant data points, and post-processing was used to calculate the battery SOH. Example cranking voltage

waveforms for battery #6 over about 40 days are shown in Figure 28. The general trends of battery aging can be observed in the figure. The July 12 and June 14 cranks are much longer because of a problem with the car engine, not the battery. Though the initial voltage is similar for each test, the valley voltages become lower as the aging proceeds. The second valley voltage is lower than the first valley for the final test on July 12. This means a negative ΔV_2, and a very low SOH. The extracted data for all batteries is in Appendix A: Battery Measurements.

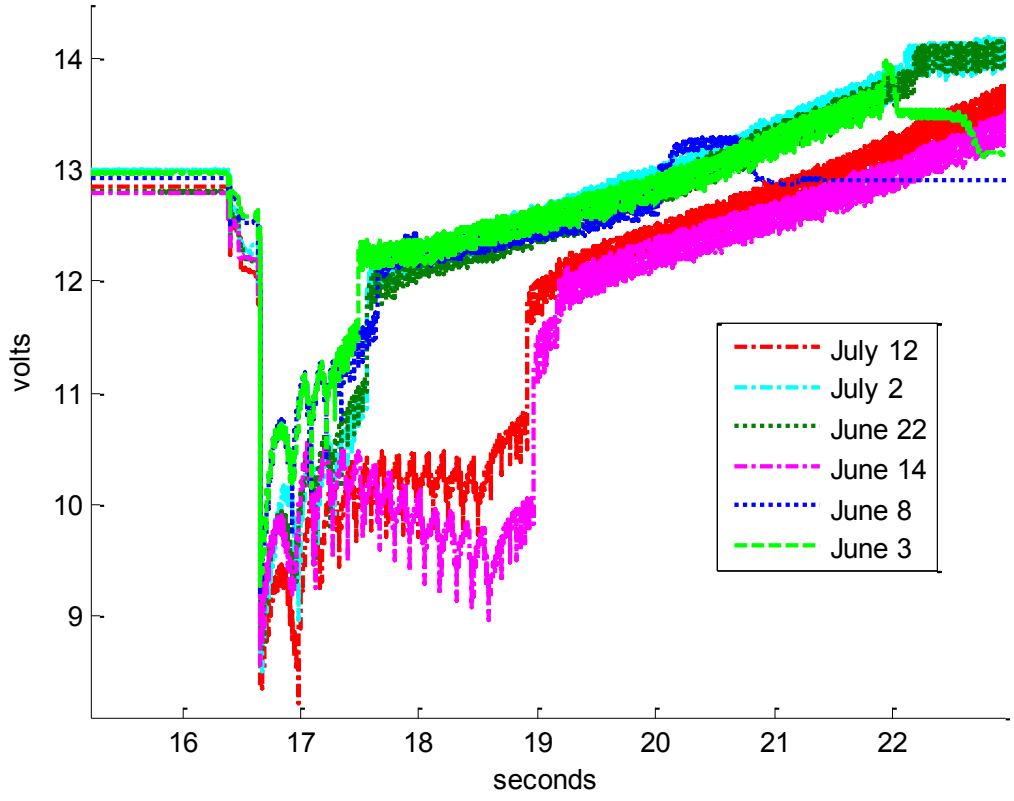

Figure 28: Crank voltage waveforms for battery #6

Table 8 shows the measured data for the waveforms given in Figure 28 and the battery temperature when the data was collected. OCV is dependent on how charged the battery is at the time of testing. On average, Valley 1 voltages become worse as the aging proceeds. In addition, Valley 2 voltages decrease. However, more striking than both of these, ΔV_1 increases and ΔV_2

decreases with age. This particular battery was very close to failure for the second test (June 8) and third test (June 14), and past failure for the fifth and sixth. For the July 2 and July 12 cranks, a warning would be given to the user that they should have their battery replaced or tested. This would allow two test-periods of warning before the failure on July 27.

Table 8: Battery #6 data extracted from crank waveforms (Year: 2014)

Measurements					ΔV		Calculated Thresholds			SOH Metric
Date	°C	OCV	Valley 1	Valley 2	ΔV_1	ΔV_2	V_{th1}	V_{th2}	V_{th}	$\Delta V_2 - V_{th}$
June 3	36	12.98	9.29	10.21	3.69	0.92	0.41	0.03	0.44	0.49
June 8	49	12.93	9.18	9.76	3.75	0.58	0.49	0.03	0.53	0.05
June 14	55	12.79	8.56	9.20	4.23	0.65	0.53	0.07	0.60	0.05
June 22	30	12.80	8.72	9.29	4.08	0.56	0.37	0.06	0.42	0.14
July 2	37	13.00	8.52	8.96	4.48	0.44	0.41	0.08	0.50	-0.05
July 12	27	12.85	8.36	8.22	4.49	-0.14	0.35	0.08	0.43	-0.57
July 27	25	12.56								failed

The final metrics for the ten batteries are shown in Table 9. Non-sequential battery numbers are due to batteries that were obtained for testing but were incapable of passing an initial crank test. The "ΔV_2 (Grube)" column shows the measured ΔV_2 from each battery test. The "SOH Metric" column shows the computed SOH metric from this work. Cells are highlighted green if their respective algorithm judged them passing, and red for failure. Though both algorithms were able to predict most battery failures, the algorithm in this work gave a better failure prediction for batteries 4, 5, and 6. A prediction is better if it is closer to the actual time of failure. The failure of Battery #13 was not predicted by either algorithm due to low SOC before its second test. All of the extracted data is in Appendix A: Battery Measurements.

Table 9: Results from ten batteries

	Battery #1		Battery #4		Battery #5	
Test #	ΔV_2 (Grube)	SOH Metric	ΔV_2 (Grube)	SOH Metric	ΔV_2 (Grube)	SOH Metric
1	0.93	0.55	0.51	0.00	1.03	0.53
2	0.98	0.46	1.19	0.64	0.90	0.22
3	0.36	-0.03	0.61	0.18		failed
4	0.63	0.22	0.11	-0.36		
5		failed		failed		
	Battery #6		Battery #7		Battery #8	
Test #	ΔV_2 (Grube)	SOH Metric	ΔV_2 (Grube)	SOH Metric	ΔV_2 (Grube)	SOH Metric
1	0.92	0.49	0.91	0.77	0.99	0.76
2	0.58	0.05	0.86	0.39	0.43	-0.01
3	0.65	0.05	0.09	-0.31		failed
4	0.56	0.14	0.06	-0.28		
5	0.44	-0.05	0.20	-0.14		
6	-0.14	-0.57				
7		failed				
	Battery #9		Battery #11		Battery #12	
Test #	ΔV_2 (Grube)	SOH Metric	ΔV_2 (Grube)	SOH Metric	ΔV_2 (Grube)	SOH Metric
1	0.44	-0.07	0.84	0.28	0.37	-0.06
2	0.54	0.16		failed	0.33	-0.16
3	0.52	0.10			0.06	-0.27
4	0.08	-0.28				failed
	Battery #13					
Test #	ΔV_2 (Grube)	SOH Metric				
1	0.81	0.33				
2		failed				

4.5 Service Life Estimate

It is an interesting and legitimate question for a driver to ask the period between the first warning from the proposed SOH monitoring system and the actual failure of the battery. The period depends on many parameters such as how often the car is driven, how long it is driven for, the weather, and through what chemical or mechanical mechanism the battery is aging. Furthermore, a battery failure is not deterministic; a battery that failed to start a car one day may be able to start the car the next day due to reasons such as temperature and engine characteristics. Therefore, it is impractical to predict the remaining battery service life accurately. So, a practical performance metric for a SOH estimator is that a battery evaluated as a failure by the estimator is also evaluated as the same when the battery is checked at a battery service center. Then, the battery should be replaced based on the warning from the SOH estimator.

Having stated the intrinsic limitation of SOH estimators above, a rough estimation of the battery life in this thesis is described as follows. Grube tested batteries with an accelerated aging technique, and his results show that a new battery failed after 12 weeks of aging [4]. Given that batteries will typically last 4-6 years, each week of aging is considered 4-6 months of real usage. In this research, the length of aging between tests was 50 to 100 hours, or approximately half that of [4]. Therefore, each period in this research can be considered two to three months. Batteries #4 and #8 gave the least amount of warning when tested, only one testing period or two to three months. Battery #7 gave three test periods of warning, and did not fail at the conclusion of testing.

5 CONCLUSION

This thesis presents a method of battery state of health monitoring which does not require current sensing. A previous method measured the difference between the first two valley voltages during a cranking event, ΔV_2 in this thesis, and compares it to a fixed threshold to determine battery health [4]. Improvements are needed to make this algorithm more reliable. Particularly, the threshold voltage should be a function of temperature. With only a fixed threshold, a battery that is close to failure but is only tested at high SOC might not give ample warning if the next crank occurs with a low SOC [4].

To mitigate the shortcomings, the proposed SOH Estimator uses the open circuit voltage, state of charge, first valley voltage (V_1), second valley voltage (V_2) and temperature (T). Consideration of temperature prevents a battery from passing consistently at high temperatures but then failing if it is operated in cold weather. The difference between the open circuit voltage and V_1 is denoted as ΔV_1 in this thesis. If ΔV_1 is very small, it is okay for ΔV_2 to also be small. Similarly, if ΔV_1 is excessive, the battery is likely unhealthy regardless of ΔV_2. When the SOC of the battery is low, both the proposed method and the existing previous method become unreliable. The proposed method avoids such a situation by performing the SOH estimation only when the SOC (which is obtained from the terminal voltage) is above 60%.

A prototype was developed that implements the proposed algorithm using an ARM processor development board. This prototype is capable of analyzing a battery's voltage during a cranking event and reporting to the driver whether the battery is healthy or not. It also serves as a data collection device that can record ambient temperature and voltage waveforms for later review.

The SOH estimation method was developed by measuring the voltage of batteries during vehicle cranking, and assessing the results. Then, additional cranks were used to validate the approach. In addition, the algorithm was implemented on a microcontroller which can be installed in a vehicle and provides feedback after each crank.

Ten batteries were used in this research to develop the algorithm thresholds and test the prototype. The batteries were held at 75° C for the duration of the aging. The aging consisted of a ten minute charging period, and then a five minute discharge period. The procedure repeated for 100 hours between testing which consists of installing the battery in a passenger car and recording a voltage waveform while starting the engine.

Both the proposed and previous algorithms were able to predict most battery failures. The algorithm in this work gave a more timely failure prediction for 30% of the batteries 4, 5, and 6. The proposed algorithm gave a failure prediction later, so the owner would get more useful time out of their battery. The other seven batteries were equally assessed.

These results confirm that the augmented algorithm is more effective at predicting battery failure. Completion of the algorithm presented in [4] by incorporating temperature-dependent thresholds was able to help avoid failure due to temperature variance. In addition, Enhancement of the algorithm presented in [4] by analyzing more points in the voltage waveform helps to more accurately predict battery end-of-life. With these two additions, the algorithm developed in this research is more strict with its thresholds and able to more finely predict when a battery will reach the end of its service life.

5.1 Future Improvements

There are numerous improvements that could be made if the SOH algorithm tracked the degradation of the battery. One such improvement is that the algorithm could measure how quickly the battery is deteriorating and then apply that same rate to predict the end of service life. Historical data will allow the SOH estimator to predict usage and environmental patterns which could then allow more accurate aging prediction.

An additional method of improving the algorithm performance would be to incorporate SOC dependent thresholds. When a battery is fully charged, its cranking waveform is closer to a healthy battery. As its SOC is lowered, the cranking waveforms are closer to that of a failing battery. Currently this is addressed by only checking the SOH if the battery has a SOC above 60%, so the thresholds are set for the case of a fully charged battery.

The algorithm performance rests completely on the detection of valley voltages in a cranking waveform. The current method analyzes the measured data with a rolling average of five data points. These averaged values should be in a “u” arrangement. The combination of a hardware low pass filter, low sampling rate, and the rolling average have reduced the chance of false detection, but relatively flat valley voltages could be missed. Though the current method worked for all tests, further investigation is recommended on this topic.

A low-SOC warning would benefit a consumer. If this warning was given, the battery should be charged by driving the vehicle frequently or through the use of an external charger. This would be immensely useful if the warning could be given remotely.

BIBLIOGRAPHY

[1] T. B. Reddy and D. Linden, Eds., *Linden's handbook of batteries*, 4th ed. New York: McGraw-Hill, 2011.

[2] D. Pavlov, *Lead-acid batteries : science and technology : a handbook of lead-acid battery technology and its influence on the product*. Amsterdam; Singapore: Elsevier Science Ltd., 2011.

[3] C.-J. Zhan, X. G. Wu, S. Kromlidis, V. K. Ramachandaramurthy, M. Barnes, N. Jenkins, and A. J. Ruddell, "Two electrical models of the lead-acid battery used in a dynamic voltage restorer," *Gener. Transm. Distrib. IEE Proc.*-, vol. 150, no. 2, pp. 175–182, 2003.

[4] R. Grube, "Automotive Battery State-Of-Health Monitoring Methods," Master of Science in Engineering, Wright State University, 2008.

[5] P. Ruetschi, "Aging mechanisms and service life of lead–acid batteries," *J. Power Sources*, vol. 127, no. 1–2, pp. 33–44, Mar. 2004.

[6] P. Ruetschi, "Energy storage and the environment: the role of battery technology," *J. Power Sources*, vol. 42, no. 1–2, pp. 1–7, Jan. 1993.

[7] D. Le and X. Tang, "Lithium-ion battery state of health estimation using ah-v characterization," in *Annual conference of the prognostics and health management society*, 2011, pp. 367–73.

[8] D. Brendt and E. Voss, *Batteries 2, Proc. of the 4th International symposium held at Brighton, U.K., Sept. 1964*, First. Pergamon Press Ltd, 1965.

[9] P. E. Pascoe and A. H. Anbuky, "Estimation of VRLS battery capacity using the analysis of the coup de fouet region," in *Telecommunication Energy Conference, 1999. INTELEC '99. The 21st International*, 1999, pp. 114–122.

[10] C. S. C. Bose and F. C. Laman, "Battery state of health estimation through coup de fouet," in *Telecommunications Energy Conference, 2000. INTELEC. Twenty-second International*, 2000, pp. 597–601.

[11] P. E. Pascoe, H. Sirisena, and A. H. Anbuky, "Coup de fouet based VRLA battery capacity estimation," in *The First IEEE International Workshop on Electronic Design, Test and Applications, 2002. Proceedings*, 2002, pp. 149–153.

[12] A. Delaille, M. Perrin, F. Huet, and L. Hernout, "Study of the 'coup de fouet' of lead-acid cells as a function of their state-of-charge and state-of-health," *J. Power Sources*, vol. 158, no. 2, pp. 1019–1028, Aug. 2006.

[13] M. Schöllmann, M. Rosenmayr, and J. Olk, "Battery Monitoring with the Intelligent Battery Sensor During Service, Standby and Production," SAE International, Warrendale, PA, SAE Technical Paper 2005-01-0561, Apr. 2005.

[14] M. Cox and K. Bertness, "Vehicle-Integrated Battery and Power System Management based on Conductance Technology to Enable Intelligent Generating Systems (inGEN®)," SAE International, Warrendale, PA, SAE Technical Paper 2001-01-2715, Nov. 2001.

[15] H. Blanke, O. Bohlen, S. Buller, R. W. De Doncker, B. Fricke, A. Hammouche, D. Linzen, M. Thele, and D. U. Sauer, "Impedance measurements on lead–acid batteries for state-of-charge, state-of-health and cranking capability prognosis in electric and hybrid electric vehicles," *J. Power Sources*, vol. 144, no. 2, pp. 418–425, Jun. 2005.

[16] O. Bohlen, S. Buller, R. W. De Doncker, M. Gelbke, and R. Naumann, "Impedance based battery diagnosis for automotive applications," in *Power Electronics Specialists Conference, 2004. PESC 04. 2004 IEEE 35th Annual*, 2004, vol. 4, pp. 2792–2797 Vol.4.

[17] X. Zhang, R. Grube, K.-K. Shin, M. Salman, and R. S. Conell, "Parity-relation-based state-of-health monitoring of lead acid batteries for automotive applications," *Control Eng. Pract.*, vol. 19, no. 6, pp. 555–563, Jun. 2011.

[18] Bosch Auto Parts, "Sensors." [Online]. Available: http://de.bosch-automotive.com/en/parts/parts_and_accessories/motor_and_sytems/start_stop_system/sensors_10/sensors_11. [Accessed: 07-Jul-2014].

[19] Hella, "INTELLIGENT BATTERY SENSOR (IBS)." [Online]. Available: http://www.hella.com/microsite-electronics/154.html?rdeLocale=en. [Accessed: 07-Jul-2014].

[20] Delphi, "Delphi IVT Battery Sensor." [Online]. Available: https://delphi.com/shared/pdf/ppd/sensors/et_ivt.pdf. [Accessed: 20-Feb-2014].

[21] Delphi, "Delphi Battery Monitoring Device." [Online]. Available: http://delphi.com/shared/pdf/ppd/ee/battery-monitoring-device.pdf. [Accessed: 20-Feb-2014].

[22] Midtronics, "MDX-600 series Battery Conductance and Electrical System Analyzer." .

[23] "Testing for Battery Drain," *Randy's Repair Shop*. [Online]. Available: http://randysrepairshop.net/testing-for-battery-drain.html. [Accessed: 14-Jul-2014].

[24] Texas Instruments, "TM4C1294NCPDT Tiva C Series Microcontroller." [Online]. Available: http://www.ti.com/product/TM4C1294NCPDT/samplebuy. [Accessed: 09-Jul-2014].

[25] Adafruit, "DS1307 Real Time Clock breakout board kit." [Online]. Available: http://www.adafruit.com/products/264. [Accessed: 10-Jul-2014].

[26] Texas Instruments, “LM34 Precision Fahrenheit Temperature Sensor.” [Online]. Available: http://www.ti.com/product/lm34. [Accessed: 10-Jul-2014].

[27] “SAE J240 Life Test for Automotive Storage Batteries.” SAE International, Dec-2012.

[28] Tractor Supply Company, “Tuff Stuff Products Heavy Duty Oval Tank, 110 gal.” [Online]. Available: http://www.tractorsupply.com/en/store/tuff-stuff-products-heavy-duty-oval-tank-110-gal. [Accessed: 10-Jul-2014].

[29] ST Micro, “VN5E010MH-E Single-channel high-side driver with analog current sense for automotive applications.” [Online]. Available: http://www.st.com/web/en/resource/technical/document/datasheet/CD00233832.pdf. [Accessed: 10-Jul-2014].

APPENDIX A: BATTERY MEASUREMENTS

IS #	Test #	date	°C	OCV	Valley 1	Valley 2	ΔV_1	ΔV_2	V_{th1}	V_{th2}	V_{th}	SOH Metric
1	1	June 3	32	12.76	9.52	10.45	3.24	0.93	0.38	0.00	0.38	0.55
	2	June 8	52	12.74	9.27	10.25	3.47	0.98	0.51	0.01	0.53	0.46
	3	June 22	30	12.47	8.77	9.14	3.70	0.36	0.37	0.03	0.40	-0.03
	4	July 2	35	12.64	9.28	9.91	3.36	0.63	0.40	0.01	0.41	0.22
	5	July 12										failed
4	1	June 8	50	12.98	9.66	10.17	3.32	0.51	0.50	0.00	0.50	0.00
	2	June 14	54	12.99	9.49	10.67	3.51	1.19	0.53	0.02	0.54	0.64
	3	June 22	30	12.45	8.28	8.89	4.17	0.61	0.37	0.06	0.43	0.18
	4	July 2	35	12.54	8.34	8.44	4.20	0.11	0.40	0.06	0.46	-0.36
	5	July 12										failed
5	1	June 8	50	12.76	9.42	10.45	3.34	1.03	0.50	0.00	0.50	0.53
	2	June 14	50	10.77	4.96	5.86	5.81	0.90	0.50	0.18	0.68	0.22
	3	June 22	30	10.16								failed
	4	July 2										failed
6	1	June 3	36	12.98	9.29	10.21	3.69	0.92	0.41	0.03	0.44	0.49
	2	June 8	49	12.93	9.18	9.76	3.75	0.58	0.49	0.03	0.53	0.05
	3	June 14	55	12.79	8.56	9.20	4.23	0.65	0.53	0.07	0.60	0.05
	4	June 22	30	12.80	8.72	9.29	4.08	0.56	0.37	0.06	0.42	0.14
	5	July 2	37	13.00	8.52	8.96	4.48	0.44	0.41	0.08	0.50	-0.05
	6	July 12	27	12.85	8.36	8.22	4.49	-0.14	0.35	0.08	0.43	-0.57
	7	July 27	25	12.56								failed
7	1	April 6		12.67	9.70	10.61	2.98	0.91	0.17	-0.02	0.14	0.77
	2	June 8	50	12.83	10.03	10.89	2.80	0.86	0.50	-0.03	0.47	0.39
	3	June 14	40	12.80	10.04	10.13	2.76	0.09	0.43	-0.04	0.40	-0.31
	4	June 22	30	12.89	10.01	10.07	2.88	0.06	0.37	-0.03	0.34	-0.28
	5	July 12	28	13.00	9.97	10.16	3.04	0.20	0.35	-0.02	0.34	-0.14
8	1	April 1	20	12.80	8.61	9.60	4.19	0.99	0.30	0.06	0.36	0.62
	2	June 1	27	12.85	8.24	8.67	4.61	0.43	0.35	0.09	0.44	-0.01
	3	June 8										failed
9	1	June 8	50	12.83	9.48	9.92	3.35	0.44	0.50	0.00	0.50	-0.07

	2	June 22	30	12.76	9.28	9.81	3.49	0.54	0.37	0.01	0.38	0.16
	3	July 2	33	12.81	9.00	9.52	3.81	0.52	0.39	0.04	0.42	0.10
	4	July 12	27	13.02	9.50	9.58	3.52	0.08	0.35	0.02	0.36	-0.28
11	1	June 8	50	12.75	8.58	9.42	4.17	0.84	0.50	0.06	0.56	0.28
	2	June 14	40	12.70					0.43			failed
	3	June 22	30	12.68								failed
12	1	June 8	45	12.91	10.21	10.58	2.70	0.37	0.47	-0.04	0.43	-0.06
	2	June 14	53	13.02	10.22	10.55	2.80	0.33	0.52	-0.03	0.49	-0.16
	3	June 22	30	12.88	10.08	10.14	2.80	0.06	0.37	-0.03	0.33	-0.27
	4	July 2										failed
13	1	June 8	50	12.81	9.769	10.58	3.04	0.81	0.50	-0.02	0.48	0.33
	2	June 14	45	10.84								failed
	3	June 22	30	12.47								failed

APPENDIX B: BATTERY IDENTIFICATION

Battery Identifier	Battery Source	Battery Description	Performance
CA 1	Campus Automotive	Rayovac	Borrowed for limited time, returned after one test
CA 2	Campus Automotive	Interstate	Borrowed for limited time, returned after one test
CA 3	Campus Automotive	Duralast	Did not hold a charge, untested.
IS 01	Interstate Batteries	Batteries Plus 75	Failed after 4 successful cranks.
IS 02	Interstate Batteries	Interstate MT-35	Did not hold a charge, untested.
IS 03	Interstate Batteries	Interstate MT-34	Did not hold a charge, untested.
IS 04	Interstate Batteries	Interstate MT-34	Failed after 4 successful cranks.
IS 05	Interstate Batteries	Autocraft 34-2	Tested, died early and did not provide significant data.
IS 06	Interstate Batteries	Econo Power Group 75	Provided 6 successful cranks, didn't die.
IS 07	Interstate Batteries	EverStart Group 34N	Provided 5 successful cranks, didn't die.
IS 08	Interstate Batteries	AAA 24F-C	Tested, died early and did not provide significant data.
IS 09	Interstate Batteries	Interstate MT-35	Provided 4 successful cranks, didn't die.
IS 10	Interstate Batteries	Autocraft MT-35	Did not hold a charge, untested.
IS 11	Interstate Batteries	Exide Group 24R	Tested, died early and did not provide significant data.
IS 12	Interstate Batteries	Duralast 34-DLG	Failed after 3 successful cranks.
IS 13	Interstate Batteries	Interstate MT-34	Tested, died early and did not provide significant data.
IS 14	Interstate Batteries	Interstate MT-35	Did not hold a charge, untested.